ACS APPLIED MATERIALS & INTERFACES

Research Article

www.acsami.org

Solvothermal Synthesis of Gallium−Indium-Zinc-Oxide Nanoparticles for Electrolyte-Gated Transistors

Lídia Santos,* Daniela Nunes, Tomás Calmeiro, Rita Branquinho, Daniela Salgueiro, Pedro Barquinha, Luís Pereira, Rodrigo Martins, and Elvira Fortunato*

Departamento de Ciência dos Materiais, CENIMAT/I3N, Faculdade de Ciências e Tecnologia, Universidade Nova de Lisboa and CEMOP/Uninova, 2829-516 Caparica, Portugal

Supporting Information

ABSTRACT: Solution-processed field-effect transistors are strategic building blocks when considering low-cost sustainable flexible electronics. Nevertheless, some challenges (e.g., processing temperature, reliability, reproducibility in large areas, and cost effectiveness) are requirements that must be surpassed in order to achieve high-performance transistors. The present work reports electrolyte-gated transistors using as channel layer gallium−indium-zinc-oxide nanoparticles produced by solvothermal synthesis combined with a solid-state electrolyte based on aqueous dispersions of vinyl acetate stabilized with cellulose derivatives, acrylic acid ester in styrene and lithium perchlorate. The devices fabricated using this approach display a I_{ON}/I_{OFF} up to 1×10^6, threshold voltage (V_{Th}) of 0.3−1.9 V, and mobility up to 1 $cm^2/(V\ s)$, as a function of gallium−indium-zinc-oxide ink formulation and two different annealing temperatures. These results validates the usage of electrolyte-gated transistors as a viable and promising alternative for nanoparticle based semiconductor devices as the electrolyte improves the interface and promotes a more efficient step coverage of the channel layer, reducing the operating voltage when compared with conventional dielectrics gating. Moreover, it is shown that by controlling the applied gate potential, the operation mechanism of the electrolyte-gated transistors can be modified from electric double layer to electrochemical doping.

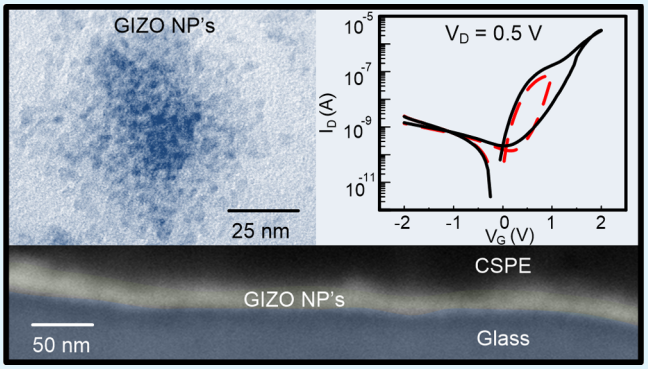

KEYWORDS: *electrolyte-gated transistor, electrochemical, electric double layer, solvothermal synthesis, GIZO nanoparticles*

1. INTRODUCTION

The aim of low-cost and sustainable devices, for a broad range of fully disposable commodities, has resulted in an increased interest in solution based deposition technologies and nanomaterials that are able to produce devices with enhanced performance and low power consumption.[1]

The first work of electrolytes used in transistors was reported in 1954 by Brattain and collaborators at Bell Laboratories.[2] At that time, the main goal was to reduce the surface defects of point contact in germanium transistors by adjusting the surface potential. Only 30 years later the use of electrolyte-gated transistors (EGTs) became popular, especially for organic transistors with the pioneer work of Wrighton et al.,[3] taking profit of the reversible electrochemical oxidation of the semiconducting polymers.

Recently, EGTs are once again attracting significant attention mainly because of the low operating voltage compared to conventional thin-film transistors (TFTs). This arises from the high capacitance of the electrolytes, usually in the order of 1−10 $\mu F\ cm^{-2}$, which exceeds the capacitance of high-κ dielectrics like Ta_2O_5 by at least 1 order of magnitude and even the one of ultrathin dielectrics based on self-assembled monolayers by a factor of ∼5.[4] Furthermore, the static capacitance of the electrolyte is nearly thickness independent, resulting in large process margins, hence in increased yield when scaling the device fabrication to industrial applications. In particular, making this type of transistors attractive for roll-to-roll printing on flexible substrates.[5] Figure 1 schematically illustrates and compares a conventional dielectric and an electrolyte-gate insulator, showing the voltage profile and the electric field distribution when a positive voltage is applied to the gate electrode.

So far, the drawbacks of the EGTs are related to large leakage currents and high switching times, as well as large parasitic capacitances, especially when integrated in an electric circuit.[4] Recent studies have been reported describing several attempts to overcome such issues nevertheless, the operation behavior of these transistors is still not fully understood. In the present study, the operation mechanism of the EGTs have been distinguished in two different types, depending on the semiconductor material permeability to ions existing in the electrolyte and on the applied gate voltage.[4] When a positive gate voltage is applied, negative and positive ions accumulate at the gate/electrolyte and

Received: October 3, 2014
Accepted: December 17, 2014
Published: December 17, 2014

DOI: 10.1021/am506814t
ACS Appl. Mater. Interfaces 2015, 7, 638−646

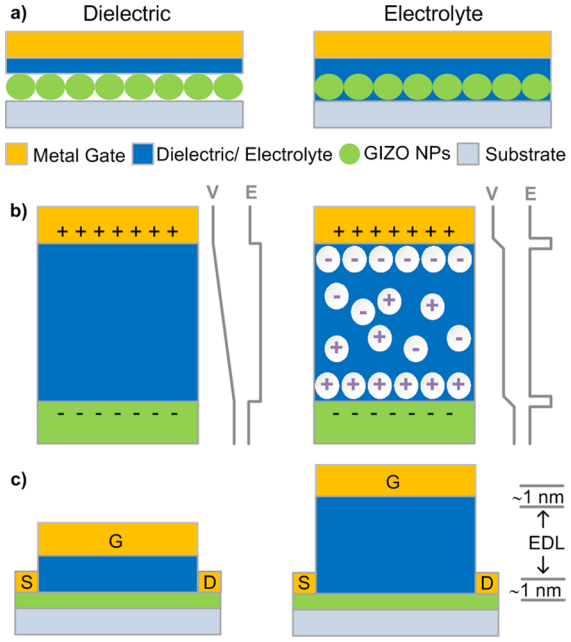

Figure 1. (a) Comparison of the cross-section of an inorganic GIZO based nanoparticles transistor using a conventional dielectric film and an electrolyte; (b) schematics of the voltage (V) and electric field (E) distributions when a positive gate voltage is applied; (c) schematics of the transistors architecture for a conventional structure incorporating thick gate dielectric (~100 nm) and for an electrolyte-gated transistor with indication of both EDLs at the gate/electrolyte and semiconductor/electrolyte interfaces.

semiconductor/electrolyte interfaces, respectively, originating two electrical double layers (EDL).[6] The charging mechanism on this type of transistors with impermeable semiconductors is similar to that of field-effect transistors, since the EDL promotes a charge carrier accumulation (or depletion) in the transistor channel (see Figure S1a in the Supporting Information). These are designed as electric double-layer transistors (EDLTs), and the active electrical thickness that enables channel modulation is in general much smaller than the geometric thickness of the electrolyte, thus resulting in a high electric field.[7]

When reversible electrochemical doping of the semiconductor (oxidation and/or reduction) occurs due to a high gate voltage or/and to the permeability of the semiconductor to ions, the electric double layer is only formed exclusively on the gate/electrolyte interface, as the ions are expected to diffuse into the semiconductor layer (see Figure S1b in the Supporting Information). This type of transistors are designed as electrochemical transistors (ECTs).[4,6] It is already known from organic ECTs,[8,9] that the ions present in the electrolyte will influence the conductivity of the channel layer. Nevertheless, the understanding of the mechanism behind this process is still under investigation, especially regarding inorganic semiconductors. From a practical point of view, EDLTs can be more interesting than ECTs as the electrochemical doping of the semiconductor can be inhibited or controlled avoiding the high leakage current normally associated with ECTs.

Oxide semiconductors are already recognized as an important class of materials for electronic applications[10] either in crystalline or amorphous structures.[11,12] One advantage of these materials is the possibility to modulate their optical and electrical properties by changing the composition and/or deposition conditions. Moreover, these materials are already being used in stable and reliable electronic devices with outstanding performances.[11] For this propose, the multicomponent oxides are interesting due to the role of the different metal cations in the conduction mechanism.[12,13] The use of sputtered gallium−indium-zinc oxide (GIZO) with different atomic ratios as semiconductor in TFTs with superior electric performance was already widely demonstrated.[12,14−16] GIZO TFTs can also be solution-processed, which has been considered as an option for low-cost fabrication. The research activities in this particular deposition method have been focused in two main routes: molecular precursor[17,18] or nanoparticles deposition.[19] For this last route, EGTs are particularly interesting as the electrolyte promotes a more efficient step coverage of the channel layer.[20]

So far, not many studies were reported regarding EGTs based in inorganic nanoparticles as semiconductors (Table 1) but mimicking the results observed with organic semiconductors, implementation of these materials in EGTs offers opportunities to improve carrier mobilities and greatly reduce operating voltages and subthreshold slope, while increasing processing tolerances and potentiating lower fabrication costs.[4]

In the present work, it has been developed GIZO nanoparticles by solvothermal synthesis with an initial atomic ratio of 2:7:1 in Ga:In:Zn, which was based on previously reported studies.[11,12] This approach is expected to result in EGTs with an acceptable compromise between low threshold voltage (V_{Th} close to 0 V) and high mobility, aiming the enhancement of the devices performance with low power consumption. To the best of the authors' knowledge, the study of the operation mechanism of inorganic EGTs by changing the ink composition, annealing temperature and applied gate voltage range has never been reported.

2. EXPERIMENTAL SECTION

2.1. Solvothermal Synthesis and Characterization of GIZO Nanoparticles. All reagents were used without further purification. Gallium nitrate hydrate ($Ga(NO_3)_3{\cdot}xH_2O$, Sigma-Aldrich, 99.9%), indium acetate ($In(CH_3COO)_3$, Sigma-Aldrich, 99.99%) and zinc acetate ($Zn(CH_3COO)_3{\cdot}2H_2O$, Sigma-Aldrich, 99.5%) were dissolved

Table 1. Key Factors of the Reported Work for EGTs with Metal Oxide Nanoparticles: Deposition Technique, Post-treatment, Electrolyte, Channel Width to Length Ratio (W/L), on−off current ratio (I_{ON}/I_{OFF}), Threshold Voltage (V_{Th}), Drain Voltage (V_D), Mobility (μ), and Subthreshold Swing (SS)

	deposition technique	post- treatment	electrolyte	W/L	I_{ON}/I_{OFF}	V_{Th} (V)	V_D (V)	μ (cm^2 (V s)$^{-1}$)	SS (V dec^{-1})
ZnO[21]	spin coating	100 °C	PVP		1×10^6	11.6	20	23.8	0.67
ZnO NR[20]	drying	150 °C	Ionic liquid	50	4×10^4	−1	1	5.5	
ZnO NW[22]	harvesting		CSPE[a]		1×10^7	0.93	0.5	62	0.12
ITO[23]	inkjet printing	400 °C	CSPE[a]	8	2×10^4	−0.22	0.8	5	
In_2O_3[24]	inkjet printing		PVA + KF	12	2×10^3	0.54	0.4	0.8−0.26	

[a]Composite solid polymer electrolyte.

DOI: 10.1021/am506814t
ACS Appl. Mater. Interfaces 2015, 7, 638−646

in 2-methoxythanol (6 mL, Fluka, 99%) with a molar ratio of 3:6:2, respectively, and left stirring at 50 °C for 1 h with ethanolamine (0.2 mL, Fluka, 98%). The final solution was transferred to a 23 mL of PTFE (polytetrafluoroethylene) chamber, set inside a stainless steel autoclave (4745 general purpose vessel, Parr) and installed in an oven (L3/11/B170, Nabertherm) at 180 °C for 24 h. The product of synthesis was collected by centrifugation at 4000 rpm for 5 min (F140, Focus instruments) and dispersed in ethanol (20 mL).

Morphological and structural characterization of GIZO nanoparticles was performed by scanning electron microscopy (SEM) combined with focused ion beam (FIB) using a Carl Zeiss AURIGA CrossBeam workstation coupled with energy-dispersive X-ray spectroscopy (EDS), and by transmission electron microscopy (TEM) using a Hitachi H8100 instrument operated at 200 kV, also equipped with EDS. For the FIB experiments the GIZO particles were previously coated with a carbon sacrificial layer, and Ga^+ ions were accelerated to 30 kV at 50 pA with an etching depth round 2 μm. The EDS was employed in 10 different samples to determine the composition of GIZO. For TEM experiments a drop of the sonicated dispersion was deposited onto 200-mesh copper grids covered with Formvar and allowed to dry before observation. X-ray diffraction (XRD) measurements have been performed using a PANalytical's X'Pert PRO MRD diffractometer with CuKα radiation. The XRD data have been acquired in the 10−70° 2θ range with a step size of 0.016°.

2.2. GIZO Thin Film Deposition and Characterization. The GIZO dispersion was mixed with ethylene glycol (Pronalab, 99.5%) in two different weight proportions (1.4:0.6 and 1.6:0.4) in order to study the ink stability and its effect on the properties of the devices. From now on, the ink with a weight fraction of EG 30% is named as GIZO30 and the ink with 20% of EG as GIZO20. Different weight fractions were also tested but the produced EGTs did not present any significant electric results (not shown). The solutions were left stirring for 24 h, and prior to deposition were sonicated for 2 min and filtered with a 0.45 μm porous diameter filter.

Glass substrates (1737, Corning) were cleaned by sonication in acetone and isopropanol and activated by UV-ozone during 30 min. Deposition of the final GIZO ink was performed by spin coating 4 layers at 2000 rpm during 35 s and rapidly drying at 100 °C for 1 min between each layer. After deposition, the substrates were annealed at 350 and 250 °C for 1 h. GIZO inks were characterized by differential scanning calorimetry and thermogravimetry (DSC-TG), accomplished directly with the solution in air with a heating ramp of 5 °C/min starting from RT up to 600 °C (STA 449 F3 Jupiter, Netzsch) while the hydrodynamic diameter was measured by dynamic light scattering (DLS) technique (W130i Avid Nano). The optical band gap was calculated from the UV−visible spectra of the deposited thin films in glass (UV/vis/NIR Lambda 950, PerkinElmer) and the surface roughness of the films was analyzed by atomic force microscopy (AFM) in a commercial microscope (Asylum research MFP-3D). The raw data were processed using planefit order 1 and flatten order 0 available in AFM software (IgorPro software). The nanoparticle size distribution was measured using Gwyddion software and scaled according to the magnification quoted by the microscope software.

2.3. Solid-Electrolyte Layer Deposition and Characterization. Composite solid polymer electrolyte (CSPE) was achieved by mixing an aqueous dispersion of acrylic acid ester in styrene stabilized with emulsifiers (pH 4, batch 2045, Resiquímica), aqueous dispersions of poly vinyl acetate (PVAc) stabilized with cellulose derivatives (pH 8, batch DM9764, Resiquímica) and lithium perchlorate ($LiClO_4$, Sigma-Aldrich, 98%). The mixture was stirred at room temperature for 1 h and deposited by spin coating at 2500 rpm during 2 min. The films were left to dry at room temperature for 8 h. Electrochemical characterization of the electrolyte was performed in a typical capacitor structure by depositing the electrolyte between two ITO-covered glass substrates (10 Ω/sq, Xinyan Technology) with an active area of 1 cm^2. Electrochemical impedance spectroscopy (EIS) was performed in a frequency range of 1 to 1 × 10^6 Hz with 10 mV AC voltage while cyclic voltammetry was achieved in a potential range between 2 and −2 V with a scan rate of 50 mV/s in a potentiostat (600TM Gamry Instruments).

2.4. Electrolyte-Gated Transistor Assembly and Characterization. Top-gated structure was achieved in several successive steps (see Figure S2 in the Supporting Information). GIZO ink was first deposited by spin coating on glass substrates. Source and drain contacts of titanium (6 nm) and gold (65 nm) metals were then e-beam evaporated (homemade apparatus) and defined with a shadow mask. The electrolyte layer (14 μm) was deposited on top by spin coating and patterned manually. The top gate of IZO (indium zinc oxide, 200 nm) was deposited by radio frequency (13.56 MHz) magnetron sputtering, using a ceramic oxide target of In_2O_3:ZnO (89.3:10.7 weight fraction, Super Conductor Materials, Inc., 99.99%). The film was deposited at room temperature in the presence of a mixture of argon (20 sccm) and oxygen (0.4 sccm) at a deposition pressure of 2 × 10^{-3} Pa with a r.f. power of 75 W and a target−substrate distance of 15 cm.[25] The patterning was achieved by mechanical shadow mask that was aligned in order to get the top-gated structure with gate-to-source and gate-to-drain overlaps of 100 μm. In this work, we used conventional electrodes made by vacuum processed techniques but fully solution-processed transistors can be achieved by replacing the contacts with conductive inks deposited by printing techniques. For FIB experiments, Ga^+ ions were accelerated to 30 kV at 2 nA and the etching depth was around 15 μm.

The electrical characterization of the transistors was performed using a semiconductor parameter analyzer (Agilent 4155C) and a microprobe station (Cascade Microtech M150) inside a dark box.

3. RESULTS AND DISCUSSION

3.1. Nanoparticle Characterization. The X-ray diffraction (XRD) measurements of the as-synthesized GIZO nanopowder is presented in Figure 2a, which is consistent with the presence of reduced-size nanoparticles because of the broad peak at 31.88°. Nevertheless, the phase determination turned to be inconclusive since the peak at 31.88° may be attributed to the presence of a nanocrystalline phase of *c*-In_2O_3[26] (ICDD file number 006−0416) or *h*-$InGaZn_2O_5$ (ICDD file number 040−0252). The crystallite size was calculated from Scherrer equation,[27] with a value of about 2.5 nm. The XRD diffractogram obtained before annealing present similarities with the characterization performed for *a*-GIZO thin films produced by pulsed-laser deposition by Nomura et al.[15] So, further analysis conducted by transmission electron microscopy (TEM) was crucial to confirm the presence of a nanocrystalline phase in our sample. The TEM image (Figure 2b) confirms the nanometric individual particles with ∼3 nm and the electron diffraction pattern (inset of Figure 2b), showing light rings together with evident diffuse halos, suggests a mixture of amorphous and nanocrystalline phases. Further annealing at 900 °C was required to distinguish the ternary mixture of oxides.

SEM observations (Figure 3a,b) illustrates the as-synthesized powder with microstructures composed of agglomerates of reduced-size nanoparticles. Only after continuous stirring and sonication, these agglomerates can be dissociated in smaller nanoparticles groups. The Energy-dispersive X-ray spectroscopy (EDS) results (Figure 3g,h) revealed an atomic ratio of 1.4:4.7:1 in Ga:In:Zn, whereas the initial fraction of the precursors before solvothermal synthesis was of 2:7:1. Even if slightly deviated, especially for indium oxide, this is in accordance with the proposed composition able to result in transistors with optimal performances.[11,12] The element mapping (Figure 3c−f) shows an even distribution of the 3 metal cations, whereas the oxygen seems to indicate a higher concentration on the surface; however, this effect can be attributed to the 3D shape of the microstructure.

The optical band gap energy calculated for the GIZO nanoparticles dispersed in ethanol resulted in 3.67 eV (see Figure S3

DOI: 10.1021/am506814t
ACS Appl. Mater. Interfaces 2015, 7, 638−646

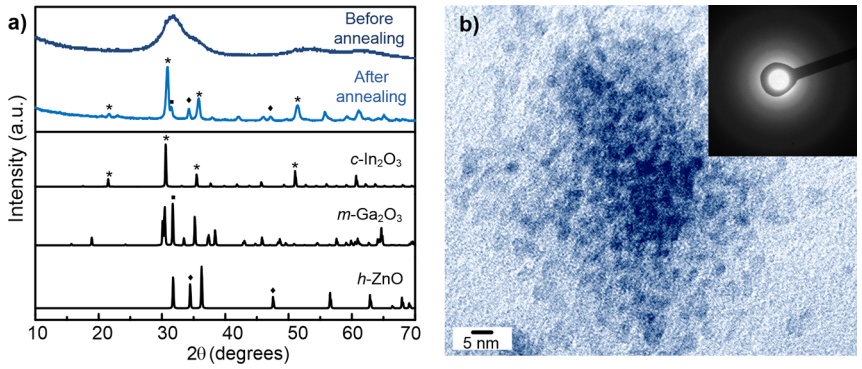

Figure 2. (a) XRD diffractograms of the synthesized GIZO nanoparticles before and after annealing at 900 °C and reference ICDD diffractograms of c-In_2O_3, m-Ga_2O_3 and h-ZnO used for comparison (file numbers 06−0416, 41−1103, and 05−0664, respectively); (b) TEM image and electron diffraction pattern of GIZO nanoparticles before annealing.

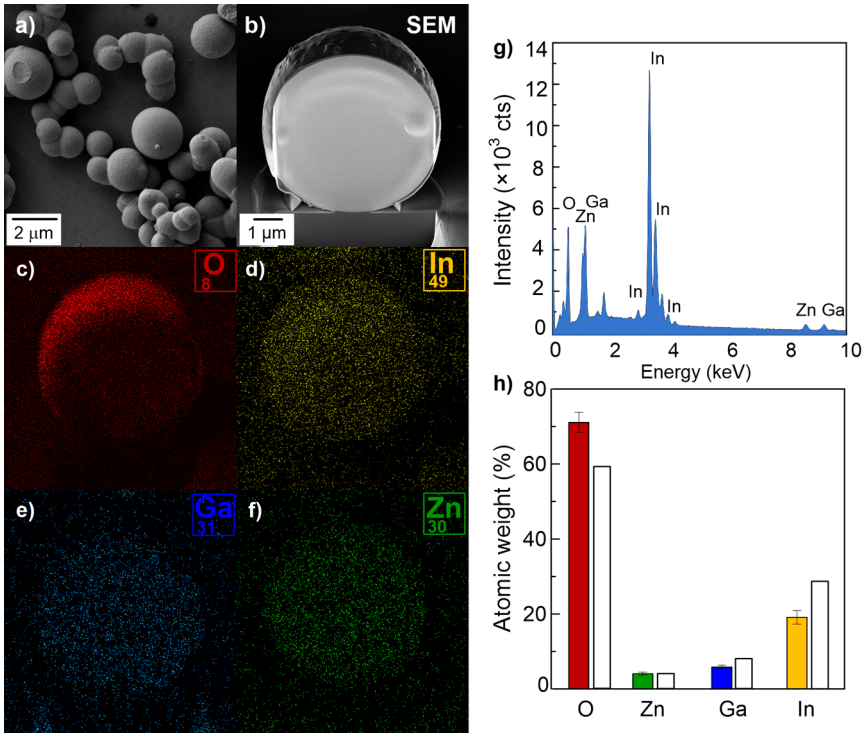

Figure 3. SEM images: (a) before and (b) after FIB milling; (c−f) EDS mapping of the elements; (g) EDS spectrum and (h) average of the atomic weights performed in 10 samples of GIZO (colored) and their percentages before synthesis (blank).

in the Supporting Information) which is in accordance with previous results of GIZO thin films produced by physical routes.[28]

3.2. GIZO Inks and Film Characterization. The two produced inks were characterized by thermogravimetry (TG) and dynamic light scattering (DLS), so that it could be estimated the size and percentage of nanoparticles after sonication and filtration processes (see Figure S4 in the Supporting Information). From the TG measurements it was observed that the GIZO nanoparticles weight fraction varied from approximately 1 to 3% for inks GIZO30 and GIZO20, respectively. The influence of the EG as dispersant can be directly related with the DLS results since the mean hydrodynamic diameter of the agglomerates decreases from 100 to 70 nm with the increase in EG proportion in the ink, thus confirming the stabilization effect of this reagent. Differential scanning calorimetry (DSC) characterization (see Figure S4b in the Supporting Information) substantiate the full degradation of the solvent and EG at 180 °C. No further peaks were verified up to 600 °C, which confirms the stable conformation of this structure.

Atomic force microscopy (AFM) measurements were performed in the substrates annealed at different temperatures (see the GIZO20 results in Figure 4). The average roughness of the films, annealed in the same conditions, varied from 9.3 to 11.7 nm for inks GIZO30 and GIZO20, respectively, and this difference is related with the ink stability and hydrodynamic diameters determined by DLS. The effect of the annealing temperature was analyzed in the phase angle images. Phase imaging provided by AFM was already demonstrated as a useful technique to distinguish features as viscoelasticity, adhesion, and contact area, because it measures the energy dissipation involved in the contact between the tip and the material analyzed.[29] In this work, the material annealed at 350 °C shows

DOI: 10.1021/am506814t
ACS Appl. Mater. Interfaces 2015, 7, 638−646

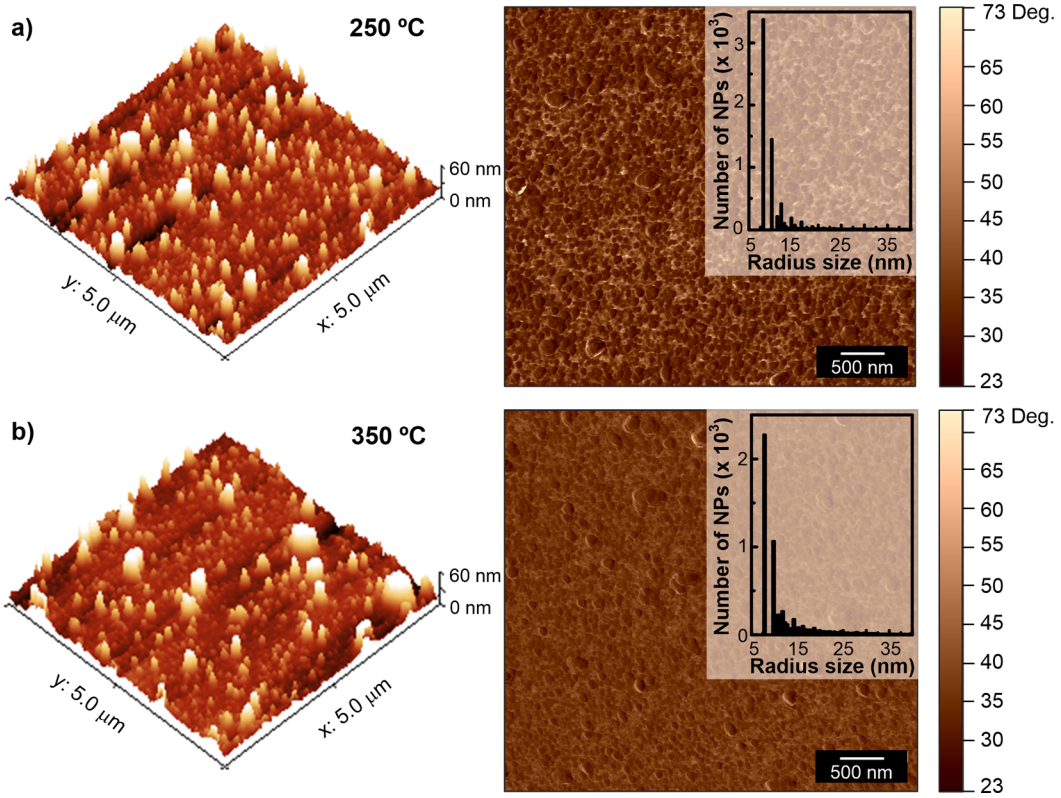

Figure 4. AFM topographic and phase images of GIZO20 films annealed at: (a) 250 and (b) 350 °C. The inset corresponds to the nanoparticles radius size distribution measured with the Gwyddion software.

a more uniform phase angle distribution when compared to the material annealed at 250 °C, which can be due to the presence of some impurities, like EG, that was not fully decomposed at lower temperature. Even if the DSC-TG characterization confirmed the full decomposition of EG at a lower temperature (180 °C), this difference can be related with heat dissipation between the hot plate and the film surface. The presence of small amounts of dispersant in the material will influence negatively on the electric and electrochemical response of the samples since it reduces the electric paths between source and drain through the GIZO nanoparticles.

AFM results also allowed the determination of the nanoparticles sizes distribution. A mean diameter of 18 nm was obtained in all measured materials, which is lower than the hydrodynamic diameters (70−100 nm) measured by DLS. This can be expected since the hydrodynamic diameter of the nanoparticles is measured in the dispersions and gives information on the inorganic core along with the solvent layer attached to the particle as it moves under the influence of Brownian motion. Thus, the AFM values are more representative of the real size of the nanoparticles. Moreover, no significant size deviations were detected between the substrates with different ink compositions and annealing temperatures.

3.3. Electrolyte Characterization. The solid electrolyte used in this work consists in a mixture of two thermoplastic polymers with $LiClO_4$, which can be easily deposited by spin coating and dried at room temperature, thus called composite solid polymer electrolyte (CSPE). Solid electrolytes are a good approach for EGTs since they can minimize and solve some of the problems associated with liquid electrolytes such as poor mechanical properties, problems in fabrication, and safety issues (leaking and hazardous environmental effects).[30−33]

The electrochemical characterization of the electrolyte was performed in a capacitor structure (ITO/electrolyte/ITO) and the impedance magnitude and phase angle were measured in the frequency range of 1 to 1 × 10^6 Hz (Figure 5a). Below 1 kHz the phase angle between current and voltage levels at around −90°, whereas at high frequencies, it gets close to zero, indicating a transition from a capacitive to a purely resistive response.[4] The transition between the two regions, at a phase angle of −45°, can be associated with the ionic relaxation and the EDL formation.[34] In the EDL formation regions, as the frequency becomes higher, the measured capacitance decreases. Accordingly, the specific capacitance obtained directly from the acquisition software also drops at higher frequencies. The frequency at which the capacitance starts to increase, is strongly dependent on the device configuration, such as size and dielectric thickness. For fast responses, this frequency value must be as high as possible.[35] When the frequency decreases to 1 Hz, the capacitance gradually increases up to 2.6 μF cm^{-2}. Even if some authors consider this value as the double-layer capacitance (C_{DL}), in the present work the value was corrected according to studies previously reported[36,37] and using the following eq 1

$$C_{DL} = [Y_0 R_s^{-(\alpha-1)}]^{1/\alpha} \quad (1)$$

where Y_0 is the bulk capacitance, R_s the solution resistance, and α is a constant (between 0 and 1). These parameters were obtained from the fitting results of the equivalent circuit (represented in Figure 5a) with a constant phase element (CPE) instead of a perfect capacitor. The resulting double layer capacitance of 0.85 μF cm^{-2} for this electrolyte is in the frontier of the usually reported values (>1 μF cm^{-2}) for electrolyte-gated transistors. Nevertheless, this CSPE was considered,

DOI: 10.1021/am506814t
ACS Appl. Mater. Interfaces 2015, 7, 638−646

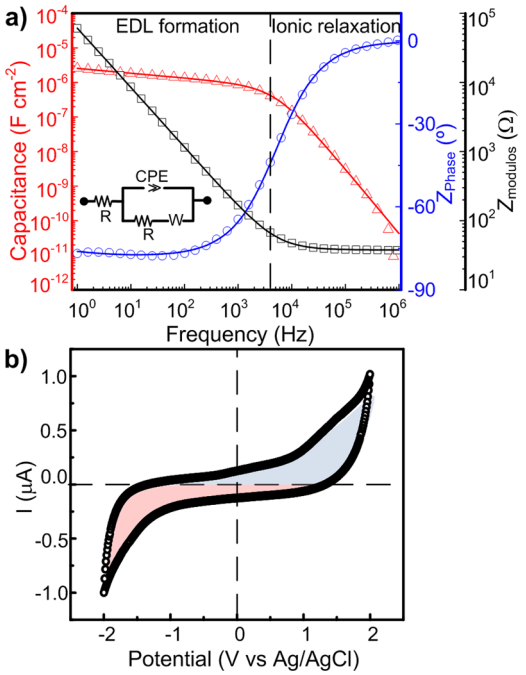

Figure 5. (a) Impedance modulus (□), phase angle (○), and capacitance (Δ) plot from EIS measurement (the inset represents the equivalent electric circuit, where R is the resistance, W the Warburg, and CPE the constant phase elements) and (b) cyclic voltammogram of ITO/electrolyte/ITO capacitor structure at a scan rate of 50 mV/s. EIS conditions: alternative voltage 10 mV and frequency range 1 to 1×10^6 Hz.

because it is compatible with solution deposition techniques allowing a good control of the layer thickness.

The conductivity was calculated according to eq 2

$$\sigma = l/(RA) \tag{2}$$

where l is the thickness of the electrolyte, A is the surface area of the sample, and R is the bulk electrical resistance (1.3×10^3 Ω), resulting in a conductivity of 1.8×10^{-6} S cm^{-1}.

Cyclic voltammetry (CV) was performed in the potential range of 2 to −2 V and the measured current is mainly capacitive with no major faradaic contribution (Figure 5b).

3.4. EGTs Characterization. Focused ion beam (FIB) experiments allowed the determination of the EGTs layers thicknesses. The analysis shows that the GIZO nanoparticles film is 30−40 nm thick and the electrolyte layer measures approximately 12 μm. Even if already demonstrated by AFM, it is visible that the GIZO nanoparticles form a continuous layer where the relatively rough surface of the nanoparticles is totally covered by the electrolyte in the channel region. The difference in the GIZO layer thickness, when using different deposition conditions, was negligible in this size range.

Electrical characterization of the EGTs was performed at room temperature and in air. The resume of the results can be found in Table 2 for the two ink compositions, two annealing temperatures, and different gate voltage ranges.

Saturation (μ_{SAT}) and linear mobilities (μ_{LIN}) were calculated accordingly with the eqs 3 and 4 for FETs[11]

$$\mu_{SAT} = \frac{\left(\frac{d\sqrt{I_D}}{dV_G}\right)^2}{\frac{1}{2}C\frac{W}{L}} \tag{3}$$

and

$$\mu_{LIN} = \frac{\left(\frac{dI_D}{dV_G}\right)}{C\frac{W}{L}V_D} \tag{4}$$

where, W/L corresponds to the width and length ratio of the channel, I_D is the drain current, V_G the gate potential, V_D drain potential, and C to the capacitance.

Subthreshold swing (SS) was given by eq 5:[11]

$$SS = \left(\frac{d\log(I_D)}{dV_G}\bigg|_{max}\right)^{-1} \tag{5}$$

EGTs produced at 250 °C, when compared with the 350 °C, required higher V_D and V_G in order to obtain I_{ON}/I_{OFF} values in the 1×10^4 to 1×10^5 range. This fact can be related with the dispersant presence (EG), as demonstrated in the AFM phase images. The EGTs annealed at 350 °C show lower V_{Th} and subthreshold swing (SS) at a considerable smaller V_G sweep (−2 to 2 V), indicative of a higher-quality channel layer. This improved performance is attributed to an enhancement of the degree of nanoparticles compactness (fully dispersant degradation and higher number of conductive paths between the nanoparticles), leading to a more homogeneous and uniform film. Moreover, the reduction of the GIZO defect density results in a lower subgap density of states and hence in an easier movement of the Fermi level toward the conduction band as V_G increases. Similar behavior was reported for GIZO TFTs prepared by physical deposition routes.[38]

For the EGTs annealed at 350 °C, the I_{ON}/I_{OFF} decreases substantially when V_G is swept between −2 and 1 V. Furthermore, the hump observed in the transfer characteristics at $V_G \approx 1$ V suggests that a different operation mechanism starts to be dominant above this V_G value. This leads to the conclusion that

Table 2. Resume of the Electric Characterization of the Produced EGTs: Channel Weight and Length Ratio (W/L), Drain Voltage (V_D), Gate Current Range (V_G), on−off Current Ratio (I_{ON}/I_{OFF}), Threshold Voltage (V_{Th}), Mobility (μ), and Subthreshold Swing (SS)

	post- treatment	W/L	V_D (V)	V_G range (V)	I_{ON}/I_{OFF}	V_{Th} (V)	μ* (cm^2 (V s)$^{-1}$)	SS* (V dec^{-1})
GIZO30	250 °C	35	1	−10 to 10	1×10^4	1.6	0.1 (μ_{SAT})	0.22
GIZO20					1×10^5	1.9	1 (μ_{SAT})	0.24
GIZO30	350 °C	15	0.5	−2 to 2	8×10^3	0.7	2×10^{-2} (μ_{LIN})	0.09
GIZO20					1×10^6	1.4	1 (μ_{LIN})	0.11
GIZO30	350 °C	15	0.5	−2 to 1	1×10^3	0.6	6×10^{-3} (μ_{LIN})	0.09
GIZO20					5×10^3	0.3	2×10^{-2} (μ_{LIN})	0.09

*Both μ and SS were calculated in the forward sweep direction, from negative to positive gate voltage.

DOI: 10.1021/am506814t
ACS Appl. Mater. Interfaces 2015, 7, 638−646

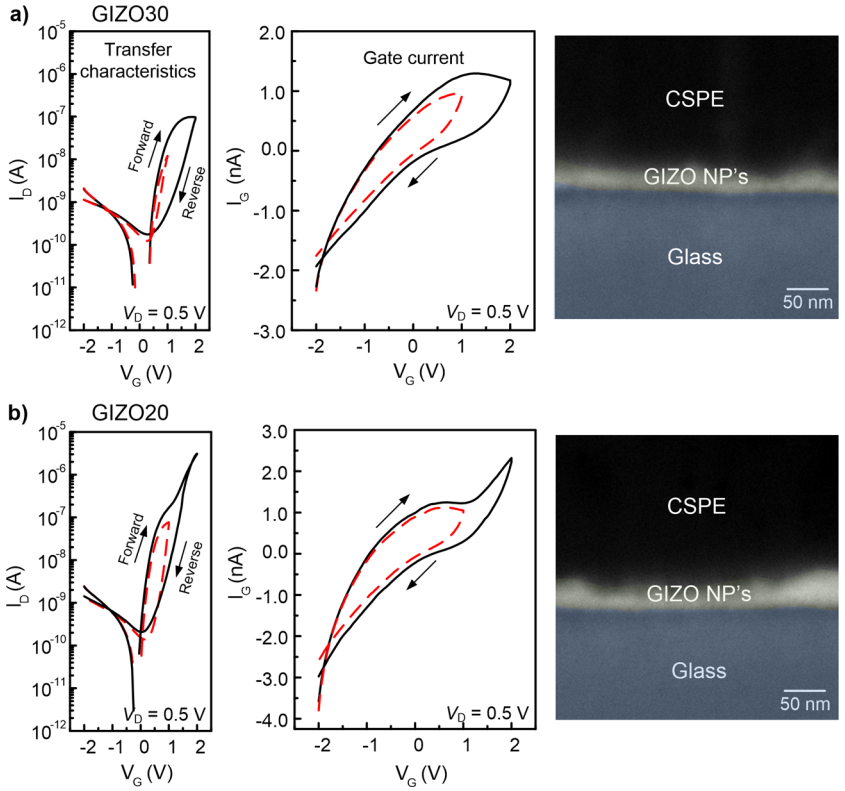

Figure 6. Transfer characteristics, gate current with different gate voltage ranges (the red dashed line corresponds to V_G from −2 to 1 V and the solid black line from −2 to 2 V) and high resolution SEM image, after FIB milling, of the cross-section of EGT built with (a) GIZO30 and (b) GIZO20 after 1 h annealing at 350 °C. Transfer characteristics and gate current were measured with 0.5 s delay time and the arrows represent the sweep direction.

the operation mechanism is different and depends on this parameter. To corroborate this conclusion, the I_G was also compared in the two operation modes. The transfer characteristics, gate current and output characteristics are shown in Figure 6. For the case of a wider V_G range, the I_G is not totally flat, which can indicate the occurrence of redox reactions and consequently doping of the semiconductor (ECT). This is more evident for the sample GIZO20, which can be related to the ink properties that generates a thicker film with more electric conduction pathways between source and drain because of the lower amount of dispersant. Nevertheless, because the gate leakage does not increase significantly, evidence of a breakdown, it suggests that this type of operation mechanism is also possible in inorganic semiconductors.[4] I_G is mainly due to the parasitic capacitance of the electrolyte, commonly observed in EGTs, and can be further minimized by changing the configuration of the transistor and by reducing the sizes of the components, like the gate-to-source and gate-to-drain overlaps.

For a narrow V_G range, from −2 to 1 V, I_G is mainly capacitive thus revealing the occurrence of electric double layer in the semiconductor/electrolyte interface (EDLTs). Nevertheless, *SS* is not expected to benefit from this operation mechanism, as it is more affected by the properties of the semiconductor film than by the occurrence of doping (redox reactions) in the interface. Thus, in the transistors annealed at 250 °C, *SS* increases due to the presence of dispersant in the films. This also suggests that the electrochemical doping of the semiconductor occurs only into few nanometers in depth and not in the bulk semiconductor.[6] Being In_2O_3 the main component of the semiconductor with a theoretical isoelectric point of 8.7,[39] the surface of the semiconductor is positively charged at the working pH from the electrolyte (below 8). This effect would also contribute for a low level of Li^+ doping (repulsive effect) into the semiconductor surface.

All produced EGTs show hysteresis of the drain current due to the slow ion motion in the solid electrolyte or to some charge trapping effects.[40] Nevertheless, the clockwise direction of the hysteresis is consistent with trapping effects that are clearly reduced in the transistors operating in EDL mode,[14] given that for the lower V_G sweep charges are only induced (not injected) in the semiconductor layer by a capacitive effect, resulting in a lower density of charges that have to be drawn during the reverse direction of the V_G sweep.

The negative differential resistance, occurring in both operation modes, suggests an adsorption process at the nanoparticle surface.[24] In addition, I_D increases with increasing V_G, confirming the n-type behavior of the GIZO nanoparticles.

Comparing with the previously reported results for EGTs based on metal oxide nanoparticles (Table 1), this results are in the same order of magnitude, but using for the first time a ternary oxide nanoparticles, which should bring advantages in terms of further device optimization, as the semiconductor properties, which are heavily dependent on the relative cationic concentration. The evaluation of the influence of the ink composition, annealing temperature and applied gate voltage allowed the discussion of the operation mechanisms that can occur in such a type of transistors.

4. CONCLUSION

In the present work, metal oxide GIZO nanoparticles were synthesized and employed as semiconductor layer, which used a

DOI: 10.1021/am506814t
ACS Appl. Mater. Interfaces 2015, 7, 638−646

composite solid polymer electrolyte as gate insulator in EGTs. The effect of the ethylene glycol as dispersant reveals the importance of achieving the right proportion in the ink formulation in order to get a stable solution, however without reducing the electric conduction paths between source and drain contacts, after ink deposition. The annealing temperature was crucial to reduce the defect density of GIZO film that allowed V_{Th} closer to 0 V with full degradation of the dispersant (ethylene glycol) and therefore, lower operating voltages. The dependence of the gate voltage in the electrical performance of the EGT was also investigated. The operation mechanism of the transistors was evaluated and it was shown evidence that the mechanism can vary from electric double layer to electrochemical doping, when increasing the gate voltage range, which allowed an improved I_{ON}/I_{OFF} and mobility values without the occurrence of voltage breakdown.

Further characterization and development of solid electrolytes and better understanding of the structure of the transistor are essential in order to improve EGTs performances. Nevertheless, this study proves that GIZO nanoparticles can easily be incorporated in EGTs compatible with solution-processed technologies, low process temperature, and flexible devices, demanded for several applications, as flexible electronics and sensors.

■ ASSOCIATED CONTENT

Supporting Information

Semiconductor/electrolyte interface of an electric double layer and electrochemical transistors. Scheme of the final transistor structure. Absorption spectra of GIZO nanoparticles dispersion. DLS and DSC-TG characterization of the GIZO inks in ethylene glycol. This material is available free of charge via the Internet at http://pubs.acs.org.

■ AUTHOR INFORMATION

Corresponding Authors

*E-mail: ls.santos@campus.fct.unl.pt.
*E-mail: emf@fct.unl.pt.

Author Contributions

The manuscript was written through contributions of all authors. All authors have given approval to the final version of the manuscript.

Notes

The authors declare no competing financial interest.

■ ACKNOWLEDGMENTS

This work was funded by the Portuguese Science Foundation (FCT-MEC) through project EXCL/CTM-NAN/0201/2012, Strategic Project PEst-C/CTM/LA0025/2013-14, "POINTS" FP7-NMP-263042, "i-FLEXIS" FP7-ICT-611070 and the FCT-MEC doctoral grant SFRH/BD/73810/2010 given to L. Santos. Moreover, this work was also supported by E. Fortunato's ERC 2008 Advanced Grant (INVISIBLE Contract 228144). The authors acknowledge Dr. Pawel Wojcik from CENIMAT/I3N for the design of the mechanical masks used in this work, Prof. P. Carvalho from Instituto Superior Técnico of Universidade de Lisboa for the TEM analysis, and Resiquímica for the polymers supply.

■ REFERENCES

(1) Martins, R.; Pereira, L.; Fortunato, E. The Future Is Paper Based. *Inf. Dispersion (1975)*. **2014**, No. 30, 20.

(2) Brattain, W. H.; Garrett, C. G. B. Electrical Properties Of The Interface Between A Germanium Single Crystal And An Electrolyte. *Phys. Rev.* **1954**, *94*, 750.

(3) White, H. S.; Kittlesen, G. P.; Wrighton, M. S. Chemical Derivatization Of An Array Of Three Gold Microelectrodes With Polypyrrole: Fabrication Of A Molecule-Based Transistor. *J. Am. Chem. Soc.* **1984**, *106*, 5375−5377.

(4) Kim, S. H.; Hong, K.; Xie, W.; Lee, K. H.; Zhang, S.; Lodge, T. P.; Frisbie, C. D. Electrolyte-gated Transistors For Organic And Printed Electronics. *Adv. Mater.* **2013**, *25*, 1822−1846.

(5) Hong, K.; Kim, S. H.; Lee, K. H.; Frisbie, C. D. Printed, Sub-2V ZnO Electrolyte Gated Transistors And Inverters On Plastic. *Adv. Mater.* **2013**, *25*, 3413−3418.

(6) Fujimoto, T.; Awaga, K. Electric-double-layer Field-effect Transistors With Ionic Liquids. *Phys. Chem. Chem. Phys.* **2013**, *15*, 8983−9006.

(7) Pereira, L.; Gaspar, D.; Guerin, D.; Delattre, a; Fortunato, E.; Martins, R. The Influence Of Fibril Composition And Dimension On The Performance Of Paper Gated Oxide Transistors. *Nanotechnology* **2014**, *25*, 094007.

(8) Yuen, J. D.; Dhoot, A. S.; Namdas, E. B.; Coates, N. E.; Heeney, M.; McCulloch, I.; Moses, D.; Heeger, A. J. Electrochemical Doping In Electrolyte-gated Polymer Transistors. *J. Am. Chem. Soc.* **2007**, *129*, 14367−14371.

(9) Kergoat, L.; Piro, B.; Berggren, M.; Horowitz, G.; Pham, M.-C. Advances In Organic Transistor-based Biosensors: From Organic Electrochemical Transistors To Electrolyte-gated Organic Field-effect Transistors. *Anal. Bioanal. Chem.* **2012**, *402*, 1813−1826.

(10) Lin, W.-N.; Ding, J.-F.; Wu, S.-X.; Li, Y.-F.; Lourembam, J.; Shannigrahi, S.; Wang, S.-J.; Wu, T. Electrostatic Modulation Of LaAlO 3 /SrTiO 3 Interface Transport In An Electric Double-Layer Transistor. *Adv. Mater. Interfaces* **2014**, *1*, 1300001.

(11) Fortunato, E.; Barquinha, P.; Martins, R. Oxide Semiconductor Thin-film Transistors: A Review Of Recent Advances. *Adv. Mater.* **2012**, *24*, 2945−2986.

(12) Olziersky, A.; Barquinha, P.; Vilà, A.; Magaña, C.; Fortunato, E.; Morante, J. R.; Martins, R. Role Of Ga2O3−In2O3−ZnO Channel Composition On The Electrical Performance Of Thin-film Transistors. *Mater. Chem. Phys.* **2011**, *131*, 512−518.

(13) Martins, R.; Barquinha, P.; Ferreira, I.; Pereira, L.; Gonçalves, G.; Fortunato, E. Role Of Order And Disorder On The Electronic Performances Of Oxide Semiconductor Thin Film Transistors. *J. Appl. Phys.* **2007**, *101*, 044505.

(14) Barquinha, P.; Pereira, L.; Gonçalves, G.; Martins, R.; Fortunato, E. Toward High-Performance Amorphous GIZO TFTs. *J. Electrochem. Soc.* **2009**, *156*, H161.

(15) Nomura, K.; Ohta, H.; Takagi, A.; Kamiya, T.; Hirano, M.; Hosono, H. Room-temperature Fabrication Of Transparent Flexible Thin-film Transistors Using Amorphous Oxide Semiconductors. *Nature* **2004**, *432*, 488−492.

(16) Suresh, A.; Wellenius, P.; Dhawan, A.; Muth, J. Room Temperature Pulsed Laser Deposited Indium Gallium Zinc Oxide Channel Based Transparent Thin Film Transistors. *Appl. Phys. Lett.* **2007**, *90*, 123512.

(17) Nayak, P. K.; Busani, T.; Elamurugu, E.; Barquinha, P.; Martins, R.; Hong, Y.; Fortunato, E. Zinc Concentration Dependence Study Of Solution Processed Amorphous Indium Gallium Zinc Oxide Thin Film Transistors Using High-k Dielectric. *Appl. Phys. Lett.* **2010**, *97*, 183504.

(18) Banger, K. K.; Yamashita, Y.; Mori, K.; Peterson, R. L.; Leedham, T.; Rickard, J.; Sirringhaus, H. Low-temperature, High-performance Solution-processed Metal Oxide Thin-film Transistors Formed By A "Sol-gel On Chip" Process. *Nat. Mater.* **2011**, *10*, 45−50.

(19) Yang, Y.-H.; Yang, S. S.; Kao, C.; Chou, K.-S. Chemical And Electrical Properties Of Low-Temperature Solution-Processed In − Ga − Zn-O Thin-Film Transistors. *IEEE Electron Device Lett.* **2010**, *31*, 329−331.

(20) Thiemann, S.; Gruber, M.; Lokteva, I.; Hirschmann, J.; Halik, M.; Zaumseil, J. High-mobility ZnO Nanorod Field-effect Transistors

DOI: 10.1021/am506814t
ACS Appl. Mater. Interfaces 2015, 7, 638−646

By Self-alignment And Electrolyte-gating. *ACS Appl. Mater. Interfaces* **2013**, *5*, 1656−1662.
(21) Faber, H.; Hirschmann, J.; Klaumünzer, M.; Braunschweig, B.; Peukert, W.; Halik, M. Impact Of Oxygen Plasma Treatment On The Device Performance Of Zinc Oxide Nanoparticle-based Thin-film Transistors. *ACS Appl. Mater. Interfaces* **2012**, *4*, 1693−1696.
(22) Nasr, B.; Wang, D.; Kruk, R.; Rösner, H.; Hahn, H.; Dasgupta, S. High-Speed, Low-Voltage, And Environmentally Stable Operation Of Electrochemically-Gated Zinc Oxide Nanowire Field-Effect Transistors. *Adv. Funct. Mater.* **2012**, *23*, 1750−1758.
(23) Dasgupta, S.; Stoesser, G.; Schweikert, N.; Hahn, R.; Dehm, S.; Kruk, R.; Hahn, H. Printed And Electrochemically Gated, High-Mobility, Inorganic Oxide Nanoparticle FETs And Their Suitability For High-Frequency Applications. *Adv. Funct. Mater.* **2012**, *22*, 4909−4919.
(24) Dasgupta, S.; Kruk, R.; Mechau, N.; Hahn, H. Inkjet Printed, High Mobility Inorganic-Oxide Field Effect Transistors Processed At Room Temperature. *ACS Nano* **2011**, *5*, 9628−9638.
(25) Gonçalves, G.; Barquinha, P.; Raniero, L.; Martins, R.; Fortunato, E. Crystallization Of Amorphous Indium Zinc Oxide Thin Films Produced By Radio-frequency Magnetron Sputtering. *Thin Solid Films* **2008**, *516*, 1374−1376.
(26) Kim, Y.-H.; Han, M.-K.; Han, J.-I.; Park, S. K. Effect Of Metallic Composition On Electrical Properties Of Solution-Processed Indium-Gallium-Zinc-Oxide Thin-Film Transistors. *IEEE Trans. Electron Devices* **2010**, *57*, 1009−1014.
(27) Koch, C. C.; Ovid'ko, I. A.; Seal, S.; Veprek, S. *Structural Nanocrystalline Materials: Fundamentals And Applications*; Cambridge University Press: Cambridge, U.K., 2007.
(28) Barquinha, P. Ph.D Thesis, Universidade Nova de Lisboa, Portugal, 2010.
(29) Eaton, P.; West, P. *Atomic Force Microscopy*; Oxford University Press: Oxford, U.K., 2010.
(30) Christie, A. M.; Lilley, S. J.; Staunton, E.; Andreev, Y. G. Increasing The Conductivity Of Crystalline Polymer Electrolytes. *Nature* **2005**, *433*, 50−53.
(31) Fan, L.-Z.; Hu, Y.-S.; Bhattacharyya, a. J.; Maier, J. Succinonitrile As A Versatile Additive For Polymer Electrolytes. *Adv. Funct. Mater.* **2007**, *17*, 2800−2807.
(32) Fergus, J. W. Ceramic And Polymeric Solid Electrolytes For Lithium-ion Batteries. *J. Power Sources* **2010**, *195*, 4554−4569.
(33) Long, S. Ionic Conduction In Doped Succinonitrile. *Solid State Ionics* **2004**, *175*, 733−738.
(34) Guo, L.-Q.; Yang, Y.-Y.; Zhu, L.-Q.; Wu, G.-D.; Zhou, J.-M.; Zhang, H.-L. Effects Of Humidity On Performance Of Electric-double-layer Oxide-based Thin-film Transistors Gated By Nanogranular SiO2 Solid Electrolyte. *AIP Adv.* **2013**, *3*, 072110.
(35) Yuan, H.; Shimotani, H.; Ye, J.; Yoon, S.; Aliah, H.; Tsukazaki, A.; Kawasaki, M.; Iwasa, Y. Electrostatic And Electrochemical Nature Of Liquid-gated Electric-double-layer Transistors Based On Oxide Semiconductors. *J. Am. Chem. Soc.* **2010**, *132*, 18402−18407.
(36) Jovic, V.; Jovic, B. M. EIS And Differential Capacitance Measurements Onto Single Crystal Faces In Different Solutions Part I: Ag (111) In 0. 01 M NaCl. *J. Electroanal. Chem.* **2003**, *541*, 1−11.
(37) Brug, G. J.; Van den Eeden, A. L. G.; Sluyters-Rehbach, M.; Sluyters, J. H. The Analysis Of Eletrode Impedances Complicated By Thepresence Of A Constant Phase Element. *J. Electroanal. Chem.* **1984**, *176*, 275−295.
(38) Kamiya, T.; Nomura, K.; Hosono, H. Present Status Of Amorphous In−Ga−Zn−O Thin-film Transistors. *Sci. Technol. Adv. Mater.* **2010**, *11*, 044305.
(39) Zhou, Y.-M.; Shan, Y.; Sun, Y.-Q.; Ju, H.-X. Adsorption Of Collagen To Indium Oxide Nanoparticles And Infrared Emissivity Study Thereon. *Mater. Res. Bull.* **2008**, *43*, 2105−2112.
(40) Kang, M. S.; Lee, J.; Norris, D. J.; Frisbie, C. D. High Carrier Densities Achieved At Low Voltages In Ambipolar PbSe Nanocrystal Thin-film Transistors. *Nano Lett.* **2009**, *9*, 3848−3852.

DOI: 10.1021/am506814t
ACS Appl. Mater. Interfaces 2015, 7, 638−646